CONF

CONF-861072--10

HELIUM TRAPPING AT Ti-RICH MC PARTICLES IN Ti-MODIFIED AUSTENITIC STAINLESS STEEL*

MASTER

P. J. Maziasz
Metals and Ceramics Division,
Oak Ridge National Laboratory, Oak Ridge, TN 37830

Helium trapping by Ti-rich MC particles is characterized by first, the formation of a high concentration of tiny cavities at the interfaces and secondly, a cavity denuded zone that extends into the surrounding matrix. Very few cavities form on other phases in the system when MC is present. The trapping is effective in HFIR from at least 370-600°C. The phases produced in unmodified steel do not exhibit this type of strong helium trapping. This trapping helps minimize the swelling for a given amount of helium. Compositionally, MC is strongly enriched in Ti, Mo, V, and Nb and depleted in Si, Ni, Cr, and Fe, both thermally and after irradiation in HFIR. The compositional behavior of MC is unusual because phases that are stabilized by irradiation are generally enriched in Si and/or Ni. The data are obtained using quantitative x-ray EDS for particles on extraction replicas. The microstructural and compositional information is examined with respect to concepts or trends from several theories to begin to understand the nature of the helium trapping.

*Research sponsored by the Office of Fusion Energy, U.S. Department of Energy, under contract No. W-7405-eng-26 with the Union Carbide Corporation.

Mechanical properties and swelling are concerns for the performance of a fusion first-wall material. Helium will be produced simultaneously with displacement damage by (n,α) reactions from 14 MeV neutrons that will be generated in the plasma. Helium can have a variety of effects, such as causing either bubble or void swelling, grain boundary embrittlement and altering phase stability in type 316 stainless steels [1–5]. Cold work has been shown effective in reducing swelling and improving mechanical properties for type 316 stainless steel irradiated in the High Flux Isotope Reactor (HFIR) which produces high levels of helium and displacement damage simultaneously [1,2]. Type 316 + 0.23 wt % Ti stainless steel (316 + Ti) is observed to have better properties than type 316 after HFIR irradiation. Reference 6 reviews both the swelling and helium embrittlement resistance obtained in several heats of titanium-modified austenites exposed to a variety of reactor or helium-producing environments. Much of the properties improvement in HFIR-irradiated (316 + Ti) is directly related to the efficient and effective trapping of helium at the MC-particle interfaces [3,5,6]. The essential experimental observations are that the MC-particles trap most or all of the helium produced in many tiny cavities located at the particle interfaces. The MC precipitate particles grow during irradiation with incorporation of little or no Si and Ni [7]. Laves particles in the same specimens incorporate considerable Ni and Si and accumulate very little helium. In this paper, the data are expanded and examined in more detail to begin to understand MC interfacial-helium trapping in terms of various theories.

Experimental

Specimens of solution-annealed (SA) 316 and either SA or 10% cold-worked (10% CW) (316 + Ti) were irradiated in HFIR at temperatures of 550 to 680°C to neutron fluences producing 1850 to 3600 at. ppm He and 30 to 57 dpa. Irradiation times ranged from about 8,000 to 16,000 h. The specimen fabrication and irradiation details are published [2,4,6–8]. Solution annealing was 1 h at 1050°C. Thermal controls from the unmachined SA rod stock of 316 were aged at 650°C for 10,000 h or 700°C for 2770 h, and (316 + Ti) was aged at 700°C for 2770 h. Alloy compositions are given in Table 1. Another heat of Ti-modified austenite was examined both in the SA condition and after homogenization at 1200°C for 24 h and then aging at 900°C for 24 h. Irradiation temperatures are calculated and they are quite reproducible, based on previous microstructural results. The actual irradiation temperatures, however, could be 50 to 75°C higher than calculated due to measurements indicating higher values of nuclear heating than initially assumed [8]. Final analysis of SiC and eutectic melt capsule monitors is pending. Helium values are calculated from an empirical relation based on mass spectrographic analysis [9]. Displacement damage levels (dpa) are calculated from the neutron fluxes and energy spectra in HFIR using the model recommended by IAEA [10].

Transmission electron microscopy (TEM) disks about 3 mm in diameter and 0.4 mm thick were cut from either gages or shoulders of tensile specimens, or from the aged pieces of rod. One disk from each specimen was thinned to electron transparency using a standard two-stage dimpling and electropolishing method [11]. A second disk from most samples was used for extracting (electrolytic etching) precipitates on an electron transparent carbon film to obtain matrix-free precipitates and eliminate the radioactive matrix (for irradiated specimens) for quantitative compositional analysis using x-ray energy dispersive spectroscopy (EDS). The details and the need for extraction replicas are reported elsewhere [7,12–14]. X-ray EDS was performed using a beryllium double-tilt holder, gimble and grid in an analytical electron microscope (AEM) (JEM 120CX) optimized for quantitative analysis [15]. Analysis was performed in the CTEM mode to minimize contamination,

Table 1. Alloy Chemistries (wt %)

	316	(316 + Ti)	Ti-Modified Austenite
Cr	18.0	17.0	14.0
Ni	13.0	12.0	16.2
Mo	2.6	2.5	2.3
Mn	1.9	0.5	1.8
Si	0.8	0.4	0.4
Ti	0.05	0.23	0.24
C	0.05	0.06	0.05
P	0.013	0.01	0.01
S	0.016	0.013	0.003
N	0.005	0.006	0.01
B	0.0005	0.0007	0.0005
V	0.01	0.01	b
Nb	0.0005	0.01	b

[a]Balance iron + trace impurities.
[b]Not detectable.

which is important when quantitatively analyzing for Si. The details of recording and analyzing the spectra on a PDP 11/34 computer, the standardless analysis technique and the constants used to deconvolute overlapping peaks are reported and discussed elsewhere [7,12–14]. Crystallographic information on the precipitate phases was obtained from selected area electron diffraction (SAD) and compared with reported data [16,17]. Bulk quantitative chemistry from the alloys used are given in Table 1 with several residual element concentrations determined by spark source mass spectroscopy (SSMS).

RESULTS

A. Microstructure

The microstructure developed during HFIR irradiation of SA 316 + Ti at 600°C to 30 dpa and 1850 at. ppm He is shown in Fig. 1. This sample was chosen for detailed study because the helium trapping by the MC particles in this microstructure is qualitatively representative of the trapping over a wide range of conditions either in HFIR or in other irradiation and/or helium producing environments [18–22]. It is on a scale that is easy to observe. Figure 1(a) shows MC particles uniformly and discretely distributed between Laves phase particles that are themselves uniformly distributed on a coarser scale. The cavity density is 2 to 3 × 10^{21} cavities/m^3 and greater than 90% of these are located at or near the MC particle interfaces. There is a cavity size gradient near the MC particles with the largest cavities being farthest from the particles. Figures 1(b) and 2 show that cavities are quite small at MC particle interfaces ranging in size from 2 to 20 nm with the distribution heavily weighted toward the smaller sizes. The cavities appear facetted and quite resistant to coalescence, particularly considering the 57 dpa exposure for the particles in Fig. 2. Figure 1(a) and (b) together show that both the surrounding matrix and the Laves particles are virtually denuded of both large and small cavities. The amount of helium necessary to balance a surface tension (γ) of 1.0 to 1.5 J/m^2 is calculated, then compared to the gas content measured for the samples assuming $P = 2\gamma/r^*$, and a Van der Waal's nonideal equation of state and integrating over the size distribution (Table 1). These ratios indicate that the cavities are either nearly equilibrium (γ = 1.5 J/m^2) or somewhat overpressured (γ = 1.0 J/m^2) bubbles. 1.0 J/m^2 is used in most theoretical studies; 1.5 J/m^2 was used because there is considerable uncertainty in surface energy values and it seemed unlikely that the bubbles were seriously overpressured.

Figure 2 shows that there are two distinct morphological variants of MC observed in irradiated (316 + Ti). SAD indicates that equiaxed particles in Fig. 2(a) have a cube-on-cube crystallographic habit relationship. MC is face centered cubic (fcc) with Herman-Mangues space group Fm3m, structure type B1 and lattice parameter a_o of about 0.43 nm [17]. The cube-on-cube

*P = gas pressure inside the cavity; r = radius of the cavity.

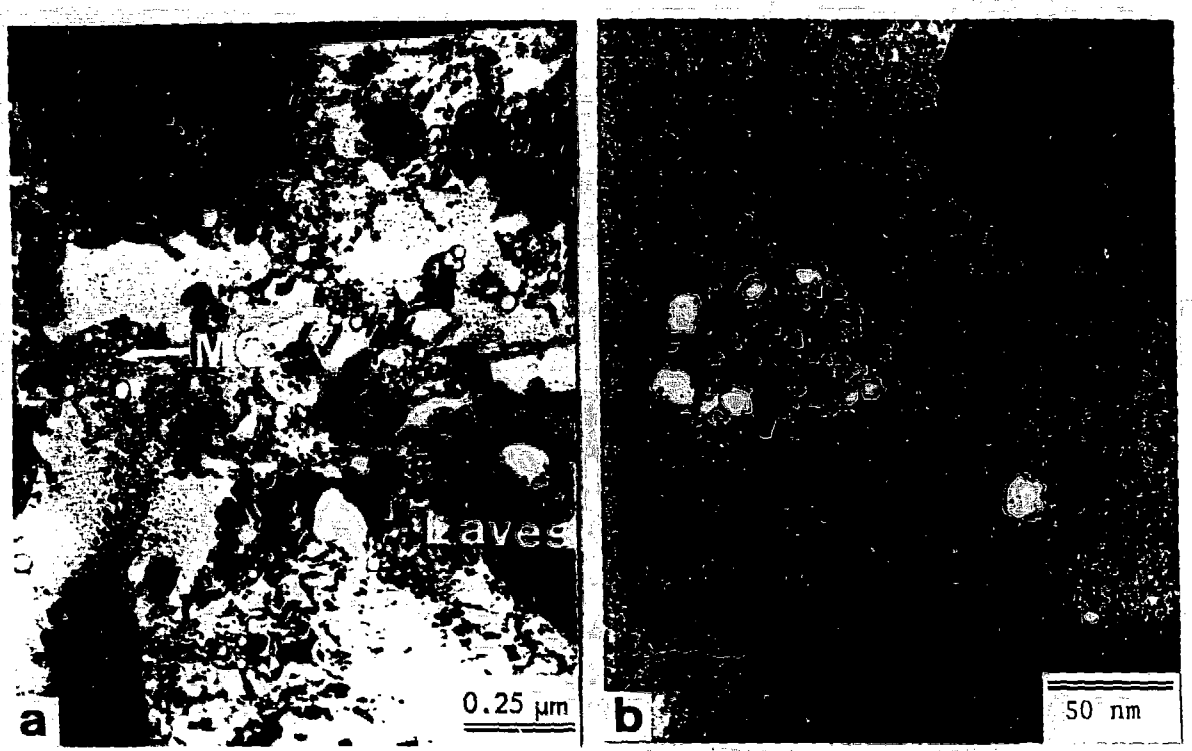

Fig. 1. TEM microstructure of SA (316 + Ti) produced by HFIR irradiation at 600°C to 30 dpa and 1850 at. ppm He. (a) Low magnification showing nearly exclusive bubble association with MC particles. (b) High magnification of MC particle with interfacial bubbles.

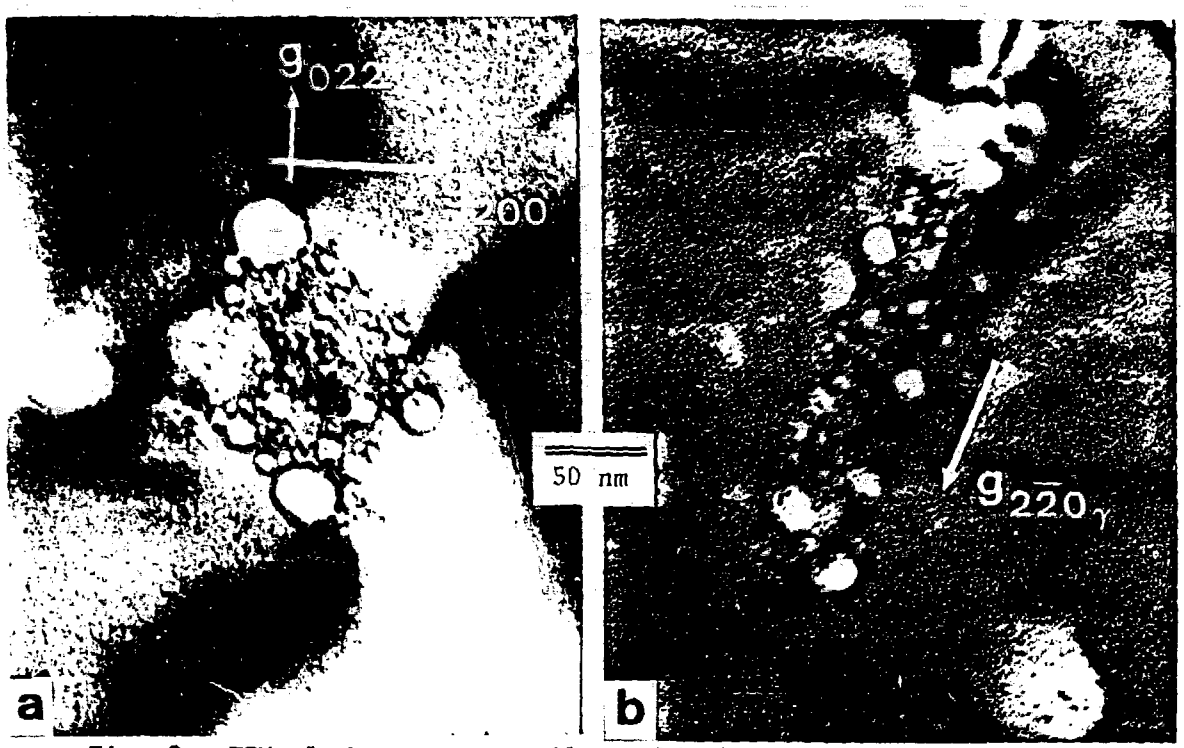

Fig. 2. TEM of the two crystallographic-habit morphological variants of MC found during HFIR irradiation of 10% CW (316 + Ti) at 610°C to 57 dpa and 3600 at. ppm He. (a) Cube-on-cube, equiaxed variant, (b) perturbed-twinned, rod-shaped variant.

crystal habit is most frequently observed for fcc phases in fcc austenite [23]. The morphology of the cube-on-cube variant appears quite similar to that characterized by Beckitt and Clark [24] for fcc $M_{23}C_6$ (tau) in austenite. The cube-on-cube variant is the only one observed in thermally aged material below 900°C [23].

The rod-shaped morphological variant of MC, shown in Fig. 2(b) is the dominant variant in SA (316 + Ti) under irradiation at these temperatures. Comparing it to the equiaxed MC variant indicates that the helium trapping is not peculiar to one variant or crystallographic interface, but rather appears to depend on the intrinsic nature of the phase. The rod variant is a new observation [7,25], but it can be produced by high-temperature aging in properly homogenized material [Fig. 3(a)]. Therefore, it is not induced by the irradiation environment but rather enhanced. The large particles of the rod variant produced thermally are easier to study than the small bubble-encrusted particles found during HFIR irradiation. Several details of the interfacial structure help explain why the fine interfacial bubble structure

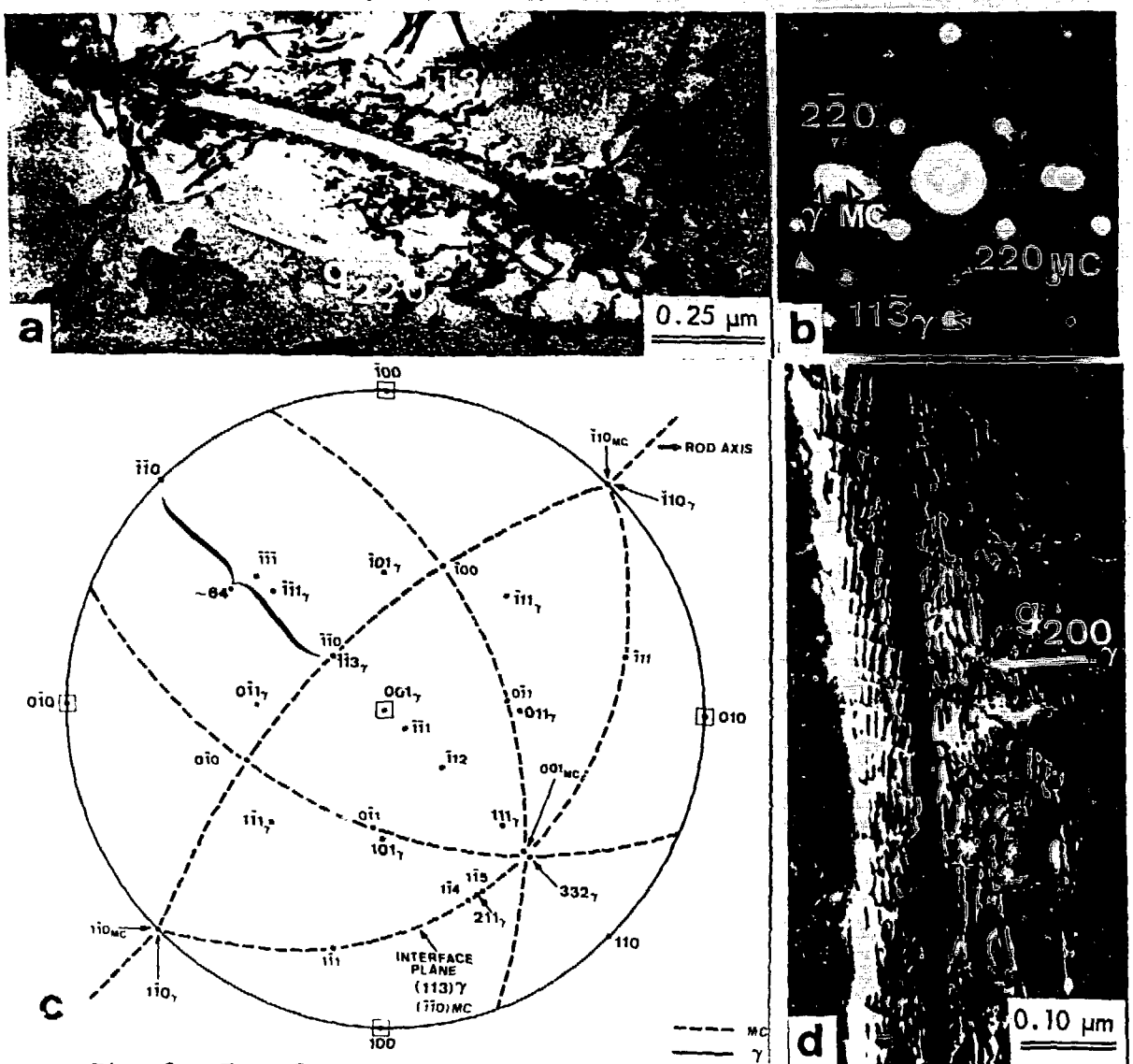

Fig. 3. TEM of the rod variant of MC produced in SA Ti-modified austenite by aging for 24 h at 900°C. (a) Bright field (BF) indicating the morphology, (b) SAD of $(332)_\gamma \| (001)_{MC}$ patterns and (c) stereographic projection, both showing the crystallographic habit and (d) weak beam dark field (WBDF) of the interfacial dislocation structure of the rod variant of MC.

nucleates and persists without coalescence. The crystallographic habit is illustrated by SAD in Fig. 3(b) and stereographically in Fig. 3(c). The habit is called a perturbed-twinned relationship because a simple counter-clockwise rotation of ~5.5° about the $[110]_\gamma \| [110]_{ppt}$ direction would result in coincidence of $(111)_\gamma \| (111)_{ppt}$ characteristic of an exact twinned relationship. There, however, appear to be good reasons for such a strange crystallographic habit. The rod axis is $[110]_\gamma [110]_{MC}$ both in Figs. 2(b) and 3(a). This habit also allows $(113)_\gamma \| (110)_{MC}$, shown in Figs. 3(b) and (c) which forms one of the broad interfaces in Fig. 3(a). An initial study of the structure of this interface [25] reveals a parallel set of dislocations with Burgers vector $[121]_\gamma$ and unit line tangent vector $(v) \| [211]_\gamma$ ($b \| [211]_\gamma$ as reported in ref. 25 is incorrect). These mixed character dislocations have the interface as their glide plane. This interface also allows every third $(332)_\gamma$ to fall within 7% of match every $(001)_{MC}$, whereas the cube-on-cube crystal habit allows every fifth plane of the austenite to come within 5% of matching every fourth MC plane of like kind on any interface. Favorable morphologies generally reflect good plane and atom matching. Interfaces with dislocation structures can be semicoherent or incoherent, but both plane matching and diffraction considerations suggest that the MC interfaces are incoherent.

The microstructure present in SA (316 + Ti) prior to HFIR irradiation is shown in Fig. 4. It contains small (20 to 40 nm in size) particles of the cube-on-cube variant of MC, nonuniformly distributed in stringers. Stringers are common in Ti-modified steels. The particle density ranges from a few in unstringered regions to about 1 to 4 × 10^{19} particles/m^3 in the stringered regions. After HFIR irradiation of (316 + Ti) at 600°C to 30 dpa the MC particle density increases to 1 to 2 × 10^{20} particles/m^3 that are fairly uniformly distributed spatially. Greater than 90% of these particles are the rod variant. Particles of both variants also are larger after irradiation (40 to 100 nm in size); therefore the volume fraction of MC has increased during irradiation. Clearly, the particles of the rod variant of MC appear to have nucleated and grown during irradiation. Many of the particles of the cube-on-cube variant may be pre-existing ones that grew during irradiation. The uniformity of the spatial distribution also means that some particles of the cube-on-cube variant may have dissolved during irradiation. The significance of the similarity of the bubble structure for the two MC variants shown in Fig. 2 is that the development of bubble-encrusted interfaces appears to depend more on MC particle presence and growth than on whether the particles nucleated prior to or during irradiation.

Comparison of the microstructure developed in SA 316 during HFIR irradiation at 575°C to 30 dpa and 2000 at. ppm He, shown in Fig. 5, helps demonstrate the efficiency and the effectiveness of helium trapping at MC particles. The only intragranular phase is Laves, and there are about 1 × 10^{16} particles/m^3. The cavity density is about 8 × 10^{19} cavities/m^3 and about 40% of these are located at the interfaces of the Laves particles. There is not much cavity denudation of the adjacent matrix, and the cavities at the Laves interfaces are about the same size as in the matrix (~ 60 nm in diameter). The large denuded zones around the MC particles and the fine cavity distribution at the interface in SA (316 + Ti) irradiated at 600°C (Fig. 1) is now striking by comparison. Laves particles, at this temperature and fluence, exhibit the best helium trapping ability, as reflected by their interfacial cavities, of any of the phases observed in HFIR irradiated unmodified 316 [2,4]. This makes the observation of almost no cavities at Laves particles in the SA (316 + Ti) (Fig. 1) quite remarkable, particularly because their number density is increased by a factor of 5 compared to the SA 316 in Fig. 5.

Fig. 4. TEM microstructure of the SA (316 + Ti) prior to either irradiation or thermal aging. The figure shows the cube-on-cube variant of MC distributed in nonuniform stringers and the high magnification inset shows their strain contrast images.

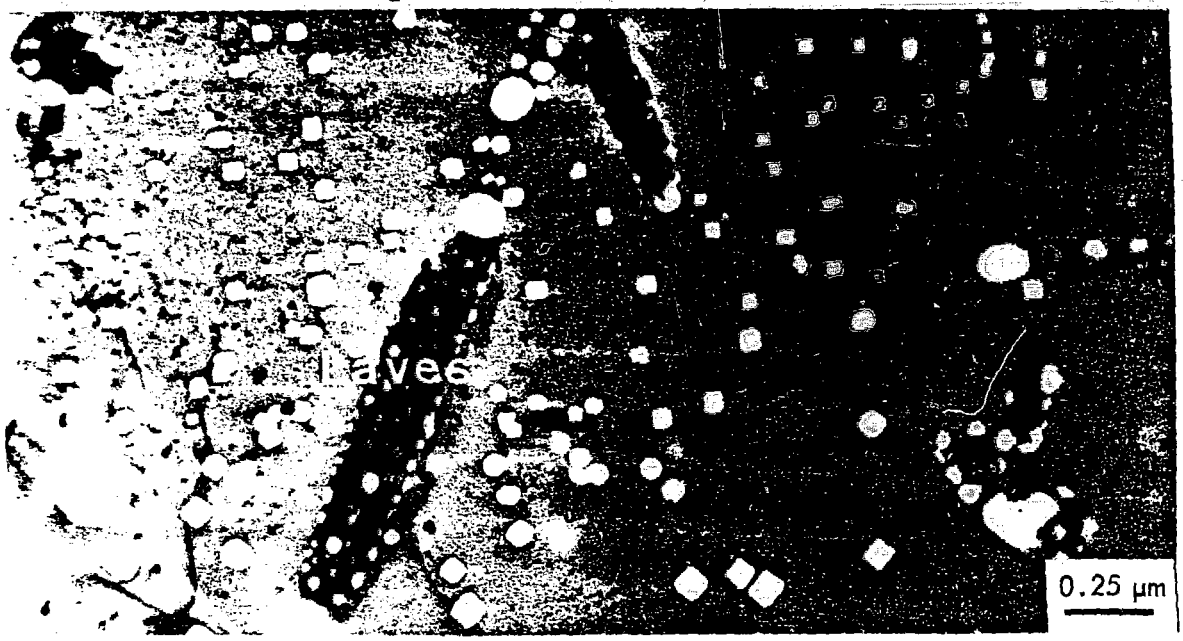

Fig. 5. TEM microstructure of SA 316 irradiated in HFIR at 575°C to 30 dpa and 2000 at. ppm He (courtesy, J. O. Stiegler).

Figure 6 compares the microstructure developed in SA (316 + Ti) irradiated in HFIR at 600°C with SA 316 and SA (316 + Ti) aged for 2770 h at 700°C. SA 316 aged at 700°C develops a slightly coarser Laves phase distribution than observed in SA (316 + Ti) after HFIR irradiation at 600°C [cf. Fig. 6(a) and (c)]. Often the Laves particles nucleate sympathetically at tau ($M_{23}C_6$) phase particles. Now, by comparison, the SA (316 + Ti) aged at 700°C has considerably less Laves than either thermally aged SA 316 or HFIR irradiated SA (316 + Ti). No Laves is observed thermally in SA (316 + Ti) at 600°C. Laves formation in thermally aged (316 + Ti) has not been reported previously [23,26].

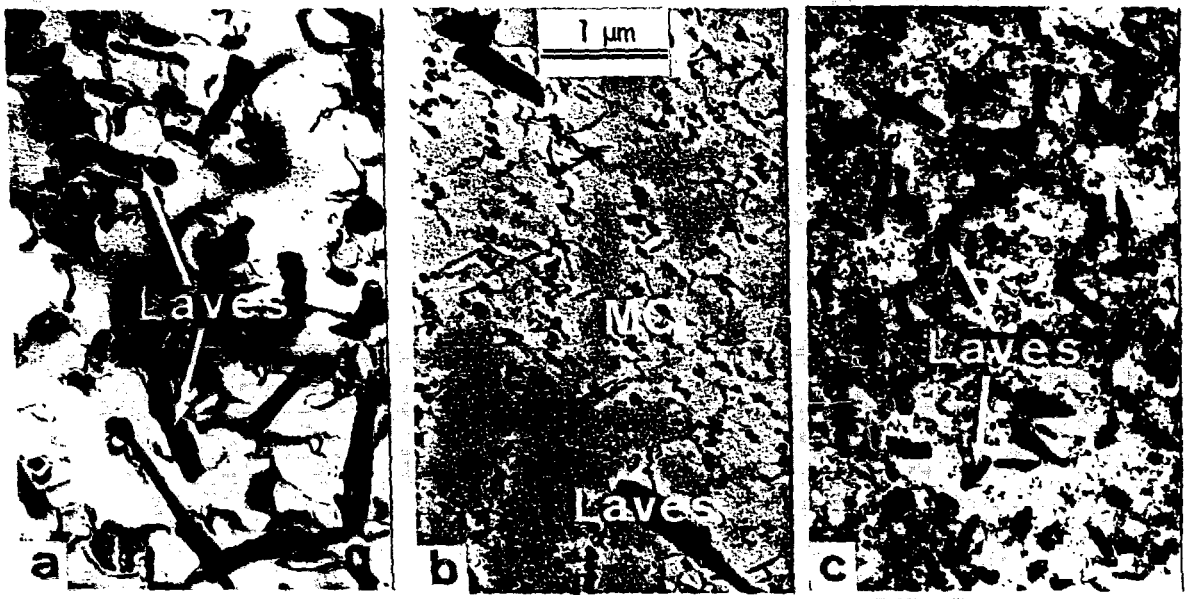

Fig. 6. TEM microstructures show Laves phase distribution for (a) SA 316 aged 2770 h at 700°C, (b) SA (316 + Ti) aged 2770 h at 700°C, and (c) SA (316 + Ti) irradiated in HFIR at 600°C to 30 dpa (12,850 h).

The Laves particles appear to develop in regions between clusters of MC particles in thermally aged SA (316 + Ti). The MC particle development in the SA (316 + Ti) is also noteworthy. The MC particle size is somewhat larger after aging compared to the starting material shown in Fig. 4, and the number density has increased considerably. In fact, these particles are only slightly coarser than those developed during HFIR irradiation in SA (316 + Ti). However, by contrast to the HFIR irradiated sample, the thermally produced particles are all the cube-on-cube variant and are clustered together rather than being discrete and spatially uniform. The thermal particles are aligned along parallel crystallographic directions within one grain and have a rather uniform size distribution. This is, however, consistent with particles emitting dislocations during growth followed by new nucleation and then subsequent growth of the new particle at the expense of the prior particle [27]. The MC particles formed in HFIR, by contrast, appear to be able to nucleate independently of one another during irradiation.

Finally, Fig. 7 is a collection of micrographs, several borrowed from other investigators, to illustrate the wide range of conditions over which MC interfacial helium trapping is observed to be effective. Figure 7(a) and (b) shows MC particles trapping helium at lower temperature and lower fluence for HFIR irradiation of the same heat of (316 + Ti) in the 20%-cold-work condition. Figure 7(c) shows a MC particle coated with small bubbles in another heat of titanium-modified steel (type 1.4970 [20]) after preinjection of 30 at. ppm He and then creep testing at 800°C and 120 mPa for 100 h (courtesy W. Kesternich [20]). Figure 7(d) shows small MC particles with interfacial bubbles developed during dual beam (4.5 pJ Si^{+6} and 0.3 pJ alpha particles) ion irradiation at 600°C and 70:1 at. ppm He/dpa to 2.5 dpa of the same heat of SA (316 + Ti) as examined in this work (courtesy S. Wood and co-workers [22]). Figure 7(e) shows again exclusive bubble trapping of helium bubbles at MC particles developed in another heat of titanium-modified austenite (SA) after EBR-II irradiation at 650°C to 39 dpa and 19 at. ppm He (courtesy E. H. Lee [21]). Obviously the MC trapping effect spans some range of damage rate, fluence, irradiation temperature, He/dpa ratio and, as shown in Fig. 7(c), can function without irradiation.

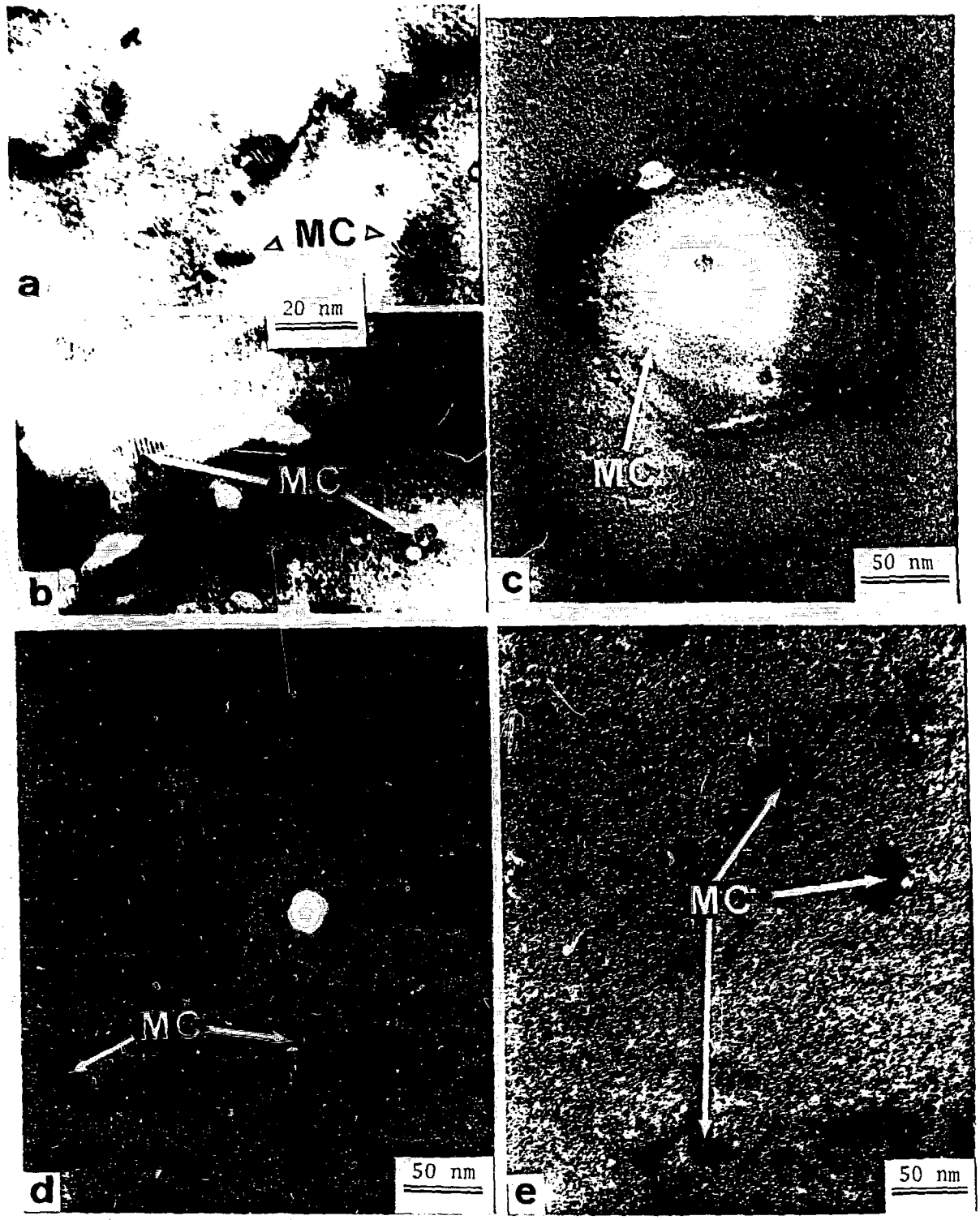

Fig. 7. TEM microstructures from several different materials to illustrate the wide range of conditions for MC interfacial trapping of helium. (a) and (b) are fine MC particles produced by HFIR irradiation of 20% CW (316 + Ti) at 375 and 565°C, respectively, to about 9–13 dpa. (c) MC in type 1.4970 stainless steel pre-injected with 30 at. ppm He and aged for 100 h at 800°C and 120 mPa (courtesy W. Kesternich [20]). (d) MC particles produced by dual ion beam irradiation of SA (316 + Ti) at 600°C and 70:1 at. ppm He/dpa to 2.5 dpa (courtesy S. Wood and co-workers [22]). (e) MC particles produced in SA Ti-modified austenite by EBR-II irradiation at 650°C to 39 dpa (courtesy E. H. Lee [21]).

B. Compositional Information

Quantitative compositional information for x-ray microanalysis of precipitates extracted on carbon replicas from various samples is given in Table 2. The primary emphasis is on SA (316 + Ti), but data from SA (Ti-modified austenite) and SA 316 are included for comparison. A small volume fraction of cube-on-cube variant MC particles is found in the SA (316 + Ti) starting material. Compared to the matrix, they are very rich in Mo, Ti, Nb, and V, and are quite depleted in Cr and Fe. They contain no detectable concentrations of Si or Mn and little or no detectable Ni. These MC particles are primarily Ti rich, containing generally 65 wt % or more Ti, and have about 20 wt % Mo. A considerably larger volume fraction of cube-on-cube MC develops during thermal aging of SA (316 + Ti) for 2770 h at 700°C together with Laves phase. Table 2 shows that MC becomes richer in Mo and poorer in Ti as the precipitation reaction progresses to a larger volume fraction in the SA (316 + Ti). The Mo content is now about 48 wt % and slightly greater than the Ti content (about 45%) [see Fig. 8(a)]. The concentrations of the other alloying elements show little change, but the Nb level is reduced. Note that there is still little or no detectable Si or

Table 2. Average Composition of Extracted Precipitate Phase Particles (wt %)

	SA (316 + Ti)			SA (Ti-Modified Austenite)	
	Unirradiated, Unaged	Aged 2770 h at 700°C		Unaged	Aged 24 h at 1200°C + 24 h at 900°C
	MC[a]	MC[b]	Laves	MC[a]	MC[b]
Si	nd	nd	3.7 ± 0.1	nd	nd
Mo	20.0 ± 4.0	48.5 ± 1.0	44.0 ± 1.0	31.0 ± 5.5	33.0
Ti	66.0 ± 3.0	43.0 ± 9.0	1.7 ± 0.1	53.0 ± 6.5	51.0
V	2.5 ± 0.7	2.0 ± 0.6	nd	3.0 ± 1.0	3.5
Cr	1.0 ± 0.5	3.5 ± 0.5	11.6 ± 0.5	3.5 ± 2.0	3.5
Mn	nd	nd	0.4 ± 0.3	1.0 ± 1.0	nd
Fe	1.0 ± 0.8	1.0 ± 1.0	33.8 ± 1.0	6.5 ± 1.0	8.0
Ni	nd to 1.0	nd to 0.5	4.8 ± 0.2	1.0 ± 0.3	1.0
Nb	9.0 ± 1.0	nd to 7.0	nd	nd to 5.4	nd

	SA (316 + Ti), HFIR 600°C 30 dpa		SA 316	
			Aged 10,000 h at 650°C	HFIR 550°C, 42 dpa
	MC[c]	Laves	Laves	Laves
Si	nd to 1.0	4.0 ± 0.5	5.0 ± 0.2	5.0
Mo	38.0 ± 4.0	31.0 ± 1.5	44.0 ± 2.0	42.0
Ti	37.0 ± 6.0	1.0 ± 0.5	nd	nd
V	5.5 ± 1.0	1.0 ± 0.5	nd	1.0
Cr	5.5 ± 0.5	16.0 ± 0.5	12.0 ± 1.5	13.5
Mn	nd	0.5 ± 0.3	0.5 ± 0.5	0.5
Fe	7.5 ± 2.5	36.5 ± 2.5	34.0 ± 1.0	30.5
Ni	3.0 ± 2.0	8.5 ± 1.0	4.5 ± 0.5	7.5
Nb	nd to 5.5	nd	nd	nd

[a]Cube-on-cube variant.
[b]Rod variant.
[c]Includes both MC variants. However, equiaxed particles have about 3 to 5 wt % Nb, whereas Nb is almost always undetectable in particles of the rod variant.

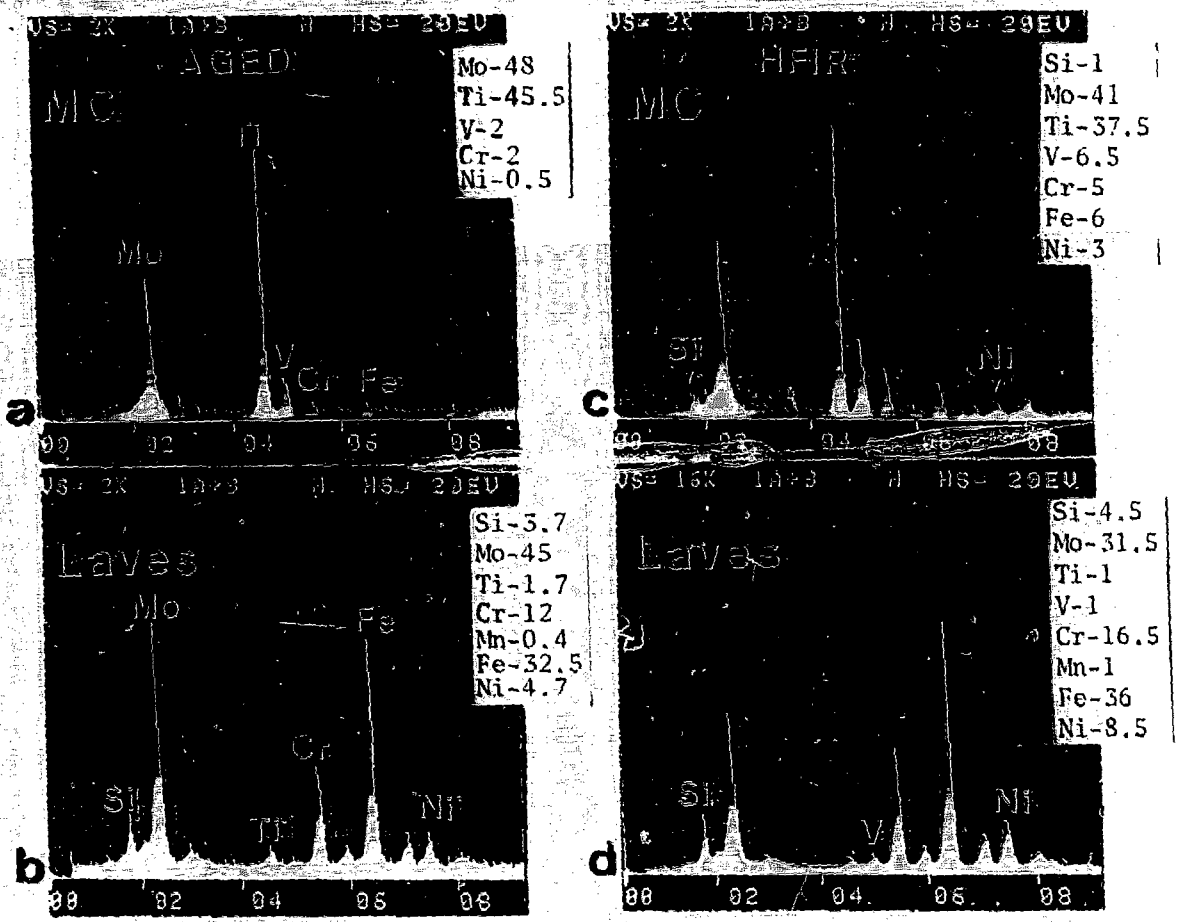

Fig. 8. Typical x-ray EDS spectra from extracted particles of (a) MC and (b) Laves produced in SA (316 + Ti) aged 2770 h at 700°C and (c) MC and (d) Laves produced in SA (316 + Ti) irradiated in HFIR at 600°C to 30 dpa. The results of quantitative compositional analysis of each spectrum are also included in weight percent.

Ni. Table 2 also shows compositional information for both fine and coarse MC particle distributions, each produced by considerably different thermal treatments, in another heat of Ti-modified austenite. The volume fraction of MC is similar for both of these heat treatments and is intermediate between the volume fractions found in the unaged and the aged SA (316 + Ti). The MC in this heat is almost identical compositionally to the MC in the (316 + Ti) particularly with respect to Ti + Mo content, and the levels of Si, Ni and the other alloying elements. The other heat of Ti-modified austenite has considerably more matrix Ni than SA (316 + Ti) (16 and 12 wt % Ni, respectively), and yet this is only slightly reflected in the MC precipitate composition. Together, these data indicate the very substantial role of Mo, Ti and other refractory elements in MC precipitation and illustrate the basic natural insolubility of the phase for the other alloying elements, particularly Si and Ni. Now, compared to this base line of thermal compositional information, Table 2 shows the MC produced in HFIR to develop along an amazingly parallel compositional path. The progression toward higher Mo and lower relative Ti with increasing volume fraction of MC is the same as the thermal behavior. The Mo + Ti content after HFIR irradiation is lower, however, than during thermal aging with significant increases in Fe and V contents and small relative increases in Cr, Ni, and Si concentrations. Of these, the most significant are the Ni and Si changes. The increases in Ni and Si concentrations in the irradiation produced MC are clearly outside the particle-to-particle variation and are still low compared to the matrix levels, particularly Ni. The lack of Ni and Si enrichments makes the MC

compositional behavior unique and pronounced compared to all the other phases produced by irradiation in stainless steel [14,28].

The compositional behavior of MC can be appreciated by observing the compositional behavior of Laves phase formed in the same material under the same thermal or irradiation conditions. In SA (316 + Ti) aged at 700°C, Table 2 shows Laves to be enriched in Si, Mo and Ti compared to the matrix. The phase has slightly less Cr and significantly less Fe and Ni than the matrix. The particle-to-particle variations in composition for Laves phases are very small. Laves phase formed in SA (316 + Ti) during aging is almost identical to Laves formed in aged SA 316, except for slightly less Si and more Ti in the former. These trends, however, are consistent with bulk matrix compositional changes of the two steels and the influence of Ti and Si on pure Laves compound formation [23,29]. Compared to thermally produced MC, Laves complements MC in its solubilities for Si, Cr, Fe, and Ni because it dissolves much more of these than does MC. Laves appears competitive with MC with respect to Mo and Ti. Now, compare Laves formed during HFIR irradiation of either SA 316 or SA (316 + Ti) at 550 to 600°C. As with the MC, the compositional development of the Laves produced during HFIR irradiation parallels almost exactly that of the thermally produced Laves phase. The higher Ni (a factor of ~ 2), slightly lower Fe and measurable V content are the only systematic perturbations in the irradiation produced phase. Comparing SA (316 + Ti) in the same fashion indicates again more Ni (a factor of 2), and slightly more Fe and Cr, measurable V, and less Mo for the irradiation-produced compared to the thermally produced phase. Again, as during thermal aging, Laves phase formation in the HFIR irradiated SA (316 + Ti) complements MC formation in its ability to dissolve more Si, Ni, Cr, and Fe than the MC phase.

DISCUSSION

We can begin to understand the MC-interfacial helium trapping by correlating the various individual microstructural and compositional observations, and then by interpreting these using concepts developed from several theories. The approach will be to consider first the MC phase by itself and then compare it to several other phases, particularly the Laves phase.

Direct TEM observations indicate that nearly all the cavities formed in the system are located at or near the MC-particle interfaces. The number density of cavities at the interface is much larger and the cavity size much smaller than those found either far away from the MC interface or in the unmodified steel. The simple gas balance equations indicate that all the gas generated could be accommodated in the cavities. A large body of theoretical and experimental work in the fundamental behavior of helium in metals indicates that the inert gas is insoluble and tends to form cavities easily when vacancies are available [30–32]. The high magnification TEM photomicrographs [Figs. 1(b), 2 and 7] clearly show no resolvable, small cavities in the matrix adjacent to the MC particles. It is therefore reasonable to conclude that nearly all the helium being generated in the system is being accumulated exclusively at the MC-particle interfaces.

By further considering the migration of helium in steel and the intrinsic nature of the MC phase, we can begin to explain this behavior of MC. Both theory and experiment appear to agree that helium atoms and vacancies can migrate together at temperatures above several hundred degrees Celsius, although there appear to be several possible mechanisms [30–32]. The binding energy of several helium atoms in vacancies is sufficient either to interfere with or to inhibit spontaneous self-interstitial recombination with the

vacancies [31]. This would make possible a slightly higher vacancy concentration when helium and displacement damage are being produced simultaneously. It may also make possible long-range migration of the helium vacancy complexes. We now need to consider why the MC particles have such an overwhelmingly biased or preferred accumulation of vacancies and helium atoms.

It is possible for precipitates to act as point defect sinks just as dislocations and grain boundaries do [33], but until recently, they have been assigned only a minor role in the development of the damage structure [34,35]. The MC phase has a large positive volume misfit with respect to the austenite matrix. On the basis of lattice parameter difference (+19.5%) for the same crystal structure (fcc), the MC phase has an increase in atomic volume/metal solute atom (av/msa) of about +70% compared to the untransformed austenite. A positive volume misfit necessitates vacancy absorption during precipitate growth [23,24,27,36], with the vacancies even being considered as a "chemical" component of the precipitate [36]. The idea of vacancy absorption by MC particles is used successfully to explain fine MC precipitation on extrinsic stacking faults during thermal aging by Silcock and Tunstall [27]. The same basic idea is considered by several workers for vacancy supersaturations stabilizing oversized misfitting phases during irradiation [37,38]. MC also has a very large, negative free energy of formation (on the order of −10 kJ/mole at ~600°C [39]) to drive the precipitate reaction [27]. Together these indicate that the MC phase is able to behave as a strongly vacancy-biased or preferring sink, particularly during the early, nonequilibrium stages of growth when the driving force is the greatest. The helium/vacancy complexes will also ensure preferred helium accumulation at a vacancy-biased sink.

If we now compare MC to some of the other phases formed in steels, we can begin to understand why the quality and magnitude of the vacancy-biased behavior of MC is unique. Both eta (M_6C) and tau ($M_{23}C_6$) phases are commonly found in 316 type steels [2–5, 14,23,24,26,28]. On the basis of their crystal structure and compound types [16,17], they are also positive volume misfitting phases, but with smaller values of av/msa of about +10%. Indeed, some phases like Laves phase (hexagonal, $P6_3/mmc$, C14, a_o = 0.47, c/a = 1.64, 12 atoms/unit cell [17]) have a slight negative volume misfit, with av/msa of about −0.05%. It becomes clear that the MC phase is unique because it has the largest positive volume misfit of the phases observed in austenitic stainless steels [23,27]. If we compare on the basis of free energy, it also appears that Ti-rich MC has one of the largest free energy driving forces of the phases observed in this type of steel [23,39].

In addition to stability, the free energy of formation also determines the solubility limits of the phase for each solute element through the chemical potential. The compositional behavior of MC reveals more information about its interaction with the point defect fluxes, especially through considering the mechanisms of radiation-induced solute segregation. Radiation-induced solute segregation theory normally predicts binding of undersized solute atoms like Ni and Si to interstitials, and then substantial enrichment of these elements at point defect sinks [40–43] (particularly interstitial sinks). The phases that are enhanced or induced in type 316 by irradiation are normally Ni and/or Si rich and their formation usually reflects a strong coupling with solute segregation. Segregation theory also predicts a significant depletion of oversized, fast diffusing alloying elements in austenite like Cr and Mo [40–45]. MC particle growth during irradiation appears to resist the normal effects of solute segregation. The MC compositional development incorporates no measurable Si and very little Ni and considerable Mo during thermal aging. The MC composition developed during irradiation is the same, except for slightly higher Si and Ni concentrations.

MC apparently has very low intrinsic solubilities for both Si and Ni. However, the large free energy driving force would be consistent with the MC phase maintaining low solubility limits for Ni and Si during irradiation. The MC phase gets additional stability during irradiation from the vacancy supersaturation and flow due to its oversized volume misfit [38]. MC formation appears to get further aid from the tremendously enhanced co-development of Laves phase particles in between clusters of MC particles during irradiation (Fig. 6). MC apparently resists interstitial absorption due both to its minimal solubilities for Si and Ni and its oversized volume misfit. Laves, by comparison, has a much greater natural solubility for both Si and Ni and has a slightly negative volume misfit and would therefore favor interstitial absorption. At the enrichment shown in Table 2, several weight percent Laves phase precipitation can account for nearly half the initial Si content in the unprecipitated matrix. A flux of mixed dumbbell interstitials in steel will also deposit a considerable amount of Fe into a phase absorbing interstitials during growth. Laves phase has the second highest natural solubility for Fe (second only to sigma phase), and MC has, by far, the lowest [14]. Both the microstructural and compositional development of Laves phase indicate a strong coupling to solute segregation by its preferred absorption of interstitial Si and Ni. Together, both the compositional and sink behavior of Laves and MC particles complement each other, making their co-development quite reasonable.

Finally, let us consider the fine bubble structure that develops at the MC-particle interfaces. This aspect of the MC-helium trapping behavior is unique. The MC particles have incoherent interfaces with a complex interfacial structure that includes dislocations, probably similar to a high-angle grain boundary. Helium is insoluble in most crystalline solids and therefore is deposited at the interface by the coupled vacancy-helium flux from the supersaturated matrix as the MC phase absorbs vacancies during particle growth. The vacancy concentration gradient depletion will maintain flow to the interface while the particle acts as a sink. Helium, however, is a powerful cavity nucleating agent [32]. The increasing helium concentration and low vacancy concentration at or adjacent to the MC-austenite interface would encourage cavity nucleation rather than cavity growth because the particle is not a sink for helium. Simple balance of the number of vacancies and gas atoms in a bubble with $2\gamma/r = P$ (all terms defined in Sect. A, Results) shows that the ratio of No. vacancies/No. gas atoms must increase proportionally to r as the cavity grows. Also, the complex interfacial structure that includes dislocations would provide abundant nucleation sites for bubbles. Taken together, these ideas appear consistent with the fine interfacial bubble structure that develops. The high concentration of possibly slightly overpressured bubbles could then continue to act as vacancy-biased sinks to maintain the flow of vacancies plus helium atoms even after the MC particles have stopped growing. Slight overpressuring seems contrary to conventional wisdom, but is consistent with their inter-competition for vacancies, their formation at a powerful vacancy-biased sink like MC, and their resistance to coalescence during irradiation [see Figs. 1(b), 2 and 7]. This explanation is satisfying because it allows the MC-helium trapping effect to be self-propagating once started, and allows it to work even without irradiation, as in the work cited by Kesternich [see Fig. 7(c)].

It is obvious that each of the subjects touched upon can and should be expanded in more depth. It is also quite obvious that with the severe embrittling effects of helium at grain boundaries, it would be of great benefit to produce particles of a phase like MC to protect the grain boundary by gathering the helium as it does in the matrix. It appears, then, that there should be considerable materials science and engineering design interest in further studying the mechanism of MC-helium interfacial trapping.

CONCLUSIONS

1. A fine distribution of cavities is observed to form exclusively at the interfaces of MC particles. It appears that most or all of the helium generated during irradiation is trapped in them.

2. MC particles formed during irradiation develop almost the same composition as do particles formed during thermal aging. In both cases, the MC contains 80 to 90 wt % (Mo + Ti) plus other refractory elements like V or Nb with little Cr, Fe, and particularly little or no Si and Ni.

3. The microstructural and compositional behavior of the MC phase is unique compared to the other phases observed in steel. These appear to be due to MC's large oversized volume misfit, large free energy driving force, and the intrinsic low solubility limit for Si and Ni.

4. The MC-helium interfacial trapping mechanism appears to involve:

(a) MC particles behaving as vacancy-biased sinks due to the oversized volume misfit,
(b) coupled co-migration of vacancies and helium atoms,
(c) minimal influence of radiation-induced solute segregation on MC formation during irradiation due to its very low Ni and Si and high Mo concentrations, indicating that MC is a very stable phase,
(d) copious bubble nucleation (and possibly slight cavity overpressuring) due to the interfacial structure and high helium and low vacancy concentrations in the matrix adjacent to the interface.

Acknowledgments

I thank E. E. Bloom, J. O. Stiegler, and F. W. Wiffen for supplying some of the HFIR irradiated specimens, and thank L. K. Mansur, A. F. Rowcliffe, J. Bentley, R. W. Carpenter and M. R. Hayns for discussion of results and theory. I thank N. J. Zaluzec, J. Bentley, E. A. Kenik, and R. W. Carpenter for the fine AEM facilities with computer without which much of this work would be impossible. I thank F. Scarboro for excellent and patient typing of the manuscript.

References

1. F. Wiffen et al., pp. 146–159 in *The Metal Science of Stainless Steels*, eds., E. W. Collings and H. W. King, TMS-AIME, New York, NY, 1979.
2. P. J. Maziasz, ibid., pp. 160–180.
3. J. A. Horak et al., pp. 325–330 in Conf. Proc. *Irradiation Behavior of Metallic Materials for Fast Reactor Core Components*, Ajaccio, Corsica, France, June 4–8, 1979.
4. P. J. Maziasz, *J. Nucl. Mater.* 85&86 (1979), 713–717.
5. P. J. Maziasz, J. A. Horak, B. L. Cox, and M. L. Grossbeck, This publication.
6. P. J. Maziasz and E. E. Bloom, to be submitted to *Journal of Nuclear Materials*, 1980.
7. P. J. Maziasz, to be published in *Scripta Metallurgica*, November 1980.
8. M. L. Grossbeck and P. J. Maziasz, *J. Nucl. Mater.* 85&86 (1979), 883–887.
9. F. W. Wiffen et al., to be submitted for publication.

10. T. A. Gabriel, B. L. Bishop, and F. W. Wiffen, *Calculated Irradiation Response of Materials Using Fission Reactors (HFIR, ORR, and EBR-II) Neutron Spectra*, Oak Ridge National Laboratory Report, ORNL/TM-6367 (August 1979).
11. C.K.H. DuBose and J. O. Stiegler, *Semiautomatic Preparation of Specimens for Transmission Electron Microscopy*, Oak Ridge National Laboratory Report, ORNL-4066 (February 1967).
12. N. J. Zaluzec, pp. 121–167 in *Introduction to Analytical Electron Microscopy*, eds. J. J. Hren, J. I. Goldstein, and D. C. Joy, Plenum Press, New York, 1979.
13. N. J. Zaluzec, this publication.
14. E. H. Lee, P. J. Maziasz, and A. F. Rowcliffe, this publication.
15. J. Bentley, N. J. Zaluzec, E. A. Kenik, and R. W. Carpenter, pp. 581–594 in *Scanning Electron Microscopy*, (Proc. Washington, D.C., April 16–20, 1979), SEM, Inc. AMF O'Hare, IL, 1979.
16. K. W. Andrews, P. J. Dryson, and S. R. Koewn, *Interpretation of Electron Diffraction Patterns*, 2nd ed., Plenum Press, New York, 1971.
17. C. J. Smithells, ed., *Metals Reference Book*, 5th ed., Butterworths, London, 1976, pp. 104–177.
18. W. R. Martin and J. R. Weir, pp. 440–456 in *Effects of Radiation on Structural Materials*, ASTM-STP 426 (1968).
19. J. P. Shepherd, *Met. Sci. J.* 3 (1969), 229–234.
20. W. Kesternich, *Trans. ANS* 33 (1979) 291.
21. E. H. Lee, Oak Ridge National Laboratory, unpublished data (1979).
22. S. Wood and J. A. Spitznagel, Westinghouse Research and Development Center, unpublished data (1980).
23. D. V. Edmonds and R.W.K. Honeycombe, pp. 121–160 in *Precipitation Processes in Solids*, TMS-AIME, eds., K. C. Russell and H. I. Aaronson, 1978, pp. 121–160.
24. F. R. Beckitt and B. R. Clark, *Acta Met.* 15 (1967), 113–129.
25. P. J. Maziasz and R. W. Carpenter, *38th Ann. Proc. Electron Microscopy Soc. Amer.*, San Francisco, CA, 1980, p. 384.
26. A. S. Grot and J. E. Spruiell, *Met. Trans. A.* 6A (1975), 2023–2030.
27. J. M. Silcock and A. W. Denham, pp. 57–64 in *Mechanisms of Phase Transformations in Crystalline Solids*, Institute of Metals Monograph and Report Series, No. 33 (1969).
28. F. A. Garner, this publication.
29. D. I. Bardos, K. P. Gupta, and P. A. Beck, *Trans. AIME* 221 (1961), 1087–1088.
30. D. E. Rimmer and A. H. Cottrell, *Phil. Mag.* 2 (1957), 1345–1353.
31. D. J. Reed, *Rad. Eff.* 31 (1977), 129–147.
32. *Harwell Consultants Symposium on Inert (Rare) Gases in Metals and Ionic Solids*, Vols. 1 and 2, ed., S. F. Pugh, AERE Harwell Report AERE-R 9733 (March 1980).
33. L. K. Mansur, *Nucl. Technol.* 40 (1978), 5–34.
34. L. K. Mansur, M. R. Hayns, and E. H. Lee, this publication.
35. L. K. Mansur, to be submitted to *Journal of Nuclear Materials* (1980).
36. K. C. Russell, *Scripta Met.* 3 (1969), 313–316.
37. P. Wilkes, *J. Nucl. Mater.* 83 (1979), 166–175.
38. K. C. Russell, *J. Nucl. Mater.* 83 (1979), 176–185.
39. S. R. Shatynski, *Oxidation of Metals* 13 (1979), 105–118.
40. P. R. Okamoto and H. Wiedersich, *J. Nucl. Mater.* 53 (1974), 336–345.
41. R. A. Johnson and N. Q. Lam, *Phys. Rev. B* 13 (1976), 4364–4375.
42. P. R. Okamoto and L. E. Rehn, *J. Nucl. Mater.* 83 (1979), 2–23.
43. H. Wiedersich, P. R. Okamoto, and N. Q. Lam, *J. Nucl. Mater.* 83 (1979), 98–108.
44. P. J. Alberry and C. W. Haworth, *Met. Sci.* 8 (1974), 407–412.
45. M. A. Krishtal and A. M. Mokrova, *Uch. Zap. Tul. Gos Pedogog. Inst., Fiz-Tekhn. Nauki* 1 (1967), 93–100.